ELSEVIER

Journal of Photochemistry and Photobiology A: Chemistry 154 (2002) 13–21

Journal of Photochemistry and Photobiology A:Chemistry

www.elsevier.com/locate/jphotochem

Intersecting-state model calculations on fast and ultrafast excited-state proton transfers in naphthols and substituted naphthols

Monica Barroso, Luis G. Arnaut, Sebastião J. Formosinho*

Departamento de Química, Universidade de Coimbra, 3049-Coimbra Codex, Portugal

Received 22 April 2002; accepted 28 June 2002

Abstract

The intersecting-state model (ISM) is applied to the calculation of absolute rate constants for proton-transfer reactions of naphthols and substituted naphthols in the first singlet state and for ground states. ISM incorporates quantum–mechanical tunnelling, zero-point energy corrections and an electrophilicity parameter to account for the lowering of the binding energy of transition states. Good agreement with experimental rates is observed over 12 orders of magnitude. The lower reactivity of the photoacids in alcohols when compared to the behaviour in water can be accounted for the differences in the potential energy curves of the OH bonds. Patterns of reactivity with respect to free-energy relations and kinetic isotope effects are also discussed.

Keywords: Excited-state proton transfer; Proton-transfer rates; Naphthol; Intersecting-state model; Kinetic isotope effects

1. Introduction

To put it in a metaphorical perspective, we aim to understand not only the structure and tectonics of the chemical reaction, but also its urbanism related with the concept of reaction families. Fifteen years after its first publication [1], the intersecting-state model (ISM) has developed into a unified theory for the understanding of fundamental concepts of chemical reactivity at both pedagogic and quantitative levels [2–5]. ISM combines the qualitative insight of structure–kinetics relationships with the quantitative approach of reaction rates theoretical chemistry.

Quantum–mechanical tunnelling, zero-point energy corrections and more quantitative electronic parameters were recently incorporated in ISM. In particular, the electronic parameter measures the electronic reshuffling attending a bond-forming–bond-breaking process. In a simple reaction of this type,

$$A + BC \rightarrow AB + C \quad (1)$$

the electronic parameter reflects the shift in electronic density between the atom (or radical) A and the atom (or radical) C when they approach the transition state configuration. A quantitative measure of the electronic reorganisation is given by an index proposed by Parr et al. [6], that we found convenient to represent by m

$$m = \frac{I + A}{I - A} \quad (2)$$

where I represents the ionisation energy and A the electronic affinity of the atom A (or C), that ranges typically between 1 and 2. When applied to stable molecules, the numerator is proportional to the absolute electronegativity and the denominator is proportional to the hardness. When I and A refer to different atoms (or radicals), the electronic parameter accounts for partial charge transfer that contributes to lowering of the binding energy of transition states.

Proton-transfer reactions both at ground and electronic excited states continue to attract a great amount of interest among theoretical chemists, both at ab initio and DFT levels. What are the sources of barrier formation or lack of it on ground state proton transfer (PT) and excited state proton transfer (ESPT)? Is there a role for charge transfer ionic valence structures in these kinds of reactions or are proton transfers better characterised as the transfer of a neutral H-atom? Does tunnelling play a significant role in the kinetic isotope effects (KIE) or are they just the result of zero-point energy differences? Do solvent molecules mediate the transfer of the proton? Those are some of the questions that we would like to address here with respect to ESPT in fast and ultrafast photoacids of naphthols and substituted

* Corresponding author. Present address: Escola Superior de Ciência e Tecnologia, Universidade Católica Portuguesa, 3504-505 Viseu, Portugal. Tel.: +351-329-852-080; fax: +351-239-827-703.
E-mail address: sformosinho@qui.uc.pt (S.J. Formosinho).

1010-6030/02/$ – see front matter
PII: S1010-6030(02)00261-7

naphthols that constitute one of the most important classes of photoacids [7].

2. ISM methodology

For a simple bond-breaking–bond-forming reaction of the kind represented by Eq. (1), reactants and products can be represented by two potential energy curves $V(n)$, displaced vertically by the reaction energy, ΔV°, and horizontally by the sum of the bond extensions of the two reactive bonds, BC and AB, as shown in Fig. 1. We use the correlation between the changes in reactant and product bond orders, to define a reaction coordinate n

$$n = n_{AB} = 1 - n_{BC} \tag{3}$$

which varies from 0 in the reactants to 1 in the products. This is identical to the reaction co-ordinate of the BEBO method [8], and is known to agree well with the actual minimum energy path for a variety of potential energy surfaces (PES) [5].

BEBO and Agmon–Levine models define energy profiles along the reaction co-ordinate where a function describing the energy dependence of a fragment (BC and AB) is multiplied by its bond order [9]. We use a similar description for our minimum energy profile,

$$V_{MEP}(n) = (1-n)V_{BC} + nV_{AB} + n\Delta V^{\circ} \tag{4}$$

The transition state is located at the maximum energy along this reaction path, $V_{max} = \Delta V^{\ddagger}$. The transition state bond order can be converted in the transition state nuclear configuration by generalising Pauling's relation [10] between bond order and bond length

$$l^{\ddagger}_{BC} - l_{BC,eq} = a'(l_{BC,eq} + l_{AB,eq})\ln(n^{\ddagger}_{BC}),$$
$$l^{\ddagger}_{AB} - l_{AB,eq} = a'(l_{BC,eq} + l_{AB,eq})\ln(n^{\ddagger}_{AB}) \tag{5}$$

The scaling by $a'(l_{BC,eq} + l_{AB,eq})$ results from the fact that longer bonds will stretch out more from equilibrium to the transition states configurations than shorter ones and that the transition state involves two bonds (BC and AB). The value of the constant a' is estimated from the PES data for $H + H_2$ reaction, $a' = 0.182$ [5].

Morse curves are realistic representations of the forces acting on the nuclei of diatomic molecules as functions of their internuclear distances, l, for configurations close to equilibrium, $l_{BC,eq}$ and $l_{AB,eq}$. For reaction (1), we will employ the Morse curves of AB and BC to obtain the minimum energy profile of Eq. (4). However, as the transition state configuration is approached, we can have an increased mixing of the wave functions describing the fragments AB and BC. When this mixing is strong, the potential energy curves are strongly rounded off in the crossing region and the height of the barrier is also strongly reduced. This effect can be accounted for by an appropriate electronic parameter, m, described before. Accordingly, the Morse curves of

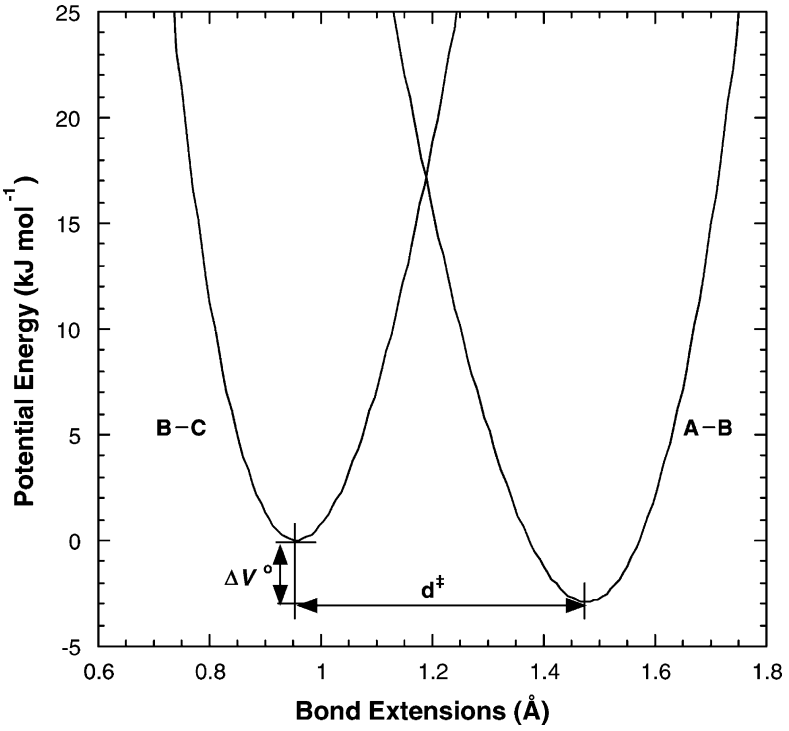

Fig. 1. ISM potential energy diagram for proton transfer of 5-cyano-2-naphthol in water; $d^{\ddagger}$ is the sum of bond extensions of reactant and product to the transition state configuration. The reaction energy ΔV° was obtained from the experimental ΔG° values, making corrections for zero-point energies, concentrations and statistical factors.

the isolated fragments must be modified to reflect the interaction between A and C as they approach each other

$$V_{BC} = D_{BC}\left[1 - \exp\left(-\frac{\beta_{BC}(l - l_{BC})}{m}\right)\right]^2,$$
$$V_{AB} = D_{AB}\left[1 - \exp\left(-\frac{\beta_{AB}(l - l_{AB})}{m}\right)\right]^2 + \Delta V^\circ \quad (6)$$

where β_{BC} and β_{AB} are the Morse coefficients of BC and AB and D_{BC} and D_{AB} the corresponding dissociation energies.

The value of $m = 1$ corresponds to the conservation of bond order along the reaction co-ordinate, assumed in the BEBO model. For a reaction in an electronic excited state, one has to take into account the electronic excitation energy, E_e, and

$$m = \frac{I - E_e + A}{I - E_e - A} \quad (7)$$

Charge-transfer structures can better represent the transition state when the value of $m = m_{CT}$, cross-estimated with an I corresponding to the atom A and A to the atom C or vice versa, is higher than that for the atom-transfer process given by Eq. (2) for a single atom or group of atoms (A or C).

The calculation of the zero-point energy of the transition state requires the vibrational frequency of the symmetric stretching and bending modes of the transition state (Fig. 2). Here we take the advantage of our knowledge of the bond order of the BC and AB fragments at the transition state to estimate their Morse parameters for the stretching mode. A detailed description of the relevant equations is presented in the Appendix A. An empirical relation for symmetric stretching and bending frequencies reveals that such frequencies are linearly related for many triatomic systems. We use this empirical relation (slope = 0.43) to get the bending frequency from the symmetric one and formulate the zero-point energy of the transition state as

$$Z_{\ddagger} = \frac{hc[\bar{\nu}_{sym} + (2 \times 0.43\bar{\nu}_{sym})]}{2} \quad (8)$$

For a vibrationally adiabatic reaction energy profile one must obtain the zero-point energy corrections along the reaction co-ordinate. With that purpose we resort to a damping function with the correct asymptotic limits for reactants, transition state and products, that interpolates from the expression of Wilson as presented in Appendix A.

Finally, proton-transfer rate constants are estimated from the transition state theory with a common frequency factor, 1×10^{10} mol^{-1} dm^3 s^{-1}. ISM views proton-transfer reactions as bimolecular processes. However, the measurement of naphthol deprotonation rates in water is usually based on the lifetimes of the corresponding singlet states, and the experimental rate constants correspond to a pseudo first-order process. In order to compare calculated and experimental rates, we estimate the reaction free energy of each elementary

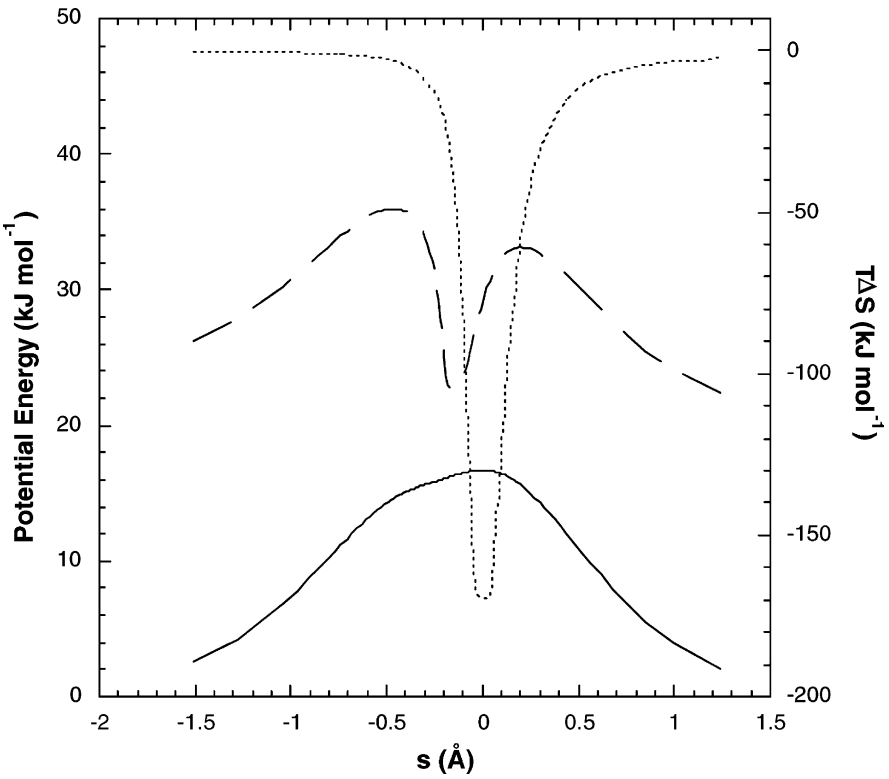

Fig. 2. Reaction energy profiles for a proton-transfer reaction. Solid line: classical energy profile; dashed line: vibrationally adiabatic energy profile; dotted line: ($T\Delta S$) profile. The reaction co-ordinate is defined as $s = \pm\sqrt{2(l_{OH} - l_{OH}^{\neq})}$.

bimolecular proton-transfer step from the experimental dynamic pK_a, corrected by statistical factors that account for the number of reactive positions available in the acid and in the base

$$\Delta G^\circ = -RT\left[2.303\mathrm{p}K_{\mathrm{AB}} + \ln\left(\frac{p_{\mathrm{B}}}{q_{\mathrm{B}}}\right) - 2.303\mathrm{p}K_{\mathrm{BC}} - \ln\left(\frac{p_{\mathrm{A}}}{q_{\mathrm{A}}}\right)\right] \quad (9)$$

where pK_{AB} refers to the base. In pure water we have p$K_{\mathrm{AB}} = -1.74$. Thus, the rate constants are given by the expression,

$$k = 10^{10}\,[\mathrm{PrAc}]\,\Gamma_{\mathrm{tunnel}}\exp\left(-\frac{\Delta H^{\ddagger}}{RT}\right) \quad (10)$$

where Γ_{tunnel} represents the tunnelling correction estimated for a Boltzmann distribution of incident particles colliding with the one-dimensional barrier of the reaction energy profile, estimated following the semi-classical approximation [11]. $\Delta H^{\ddagger}$ represents the enthalpy of activation,

$$\Delta H^{\ddagger} = \Delta V^{\ddagger} - \Delta Z^{\ddagger} - RT \quad (11)$$

$\Delta Z^{\ddagger}$ the zero-point energy difference between transition state and reactants, and [PrAc] the concentration of the proton acceptor in solution. For example, for proton transfers to water molecules in water [PrAc] = 55.6 mol dm^{-3} and in methanol [PrAc] = 24.7 mol dm^{-3}.

3. Calculations

3.1. Naphthols

1-Naphthol has long been considered a model of a strong photoacid when excited to the first electronic singlet state S_1. Pines et al. [12] have studied the photo-dissociation of 1-naphthol in water that occurs at room temperature with a lifetime of about 36 ps, assuming a unidirectional dissociation reaction. In D_2O the lifetime is 117 ps at 23 °C and KIE = 3.25. The ion-pair which is generated by the proton dissociation may separate by diffusion or recombine geminately. At the same time the base form undergoes irreversible geminate quenching reaction.

For the proton-transfer reaction in 1-naphtol in water, the reactive bonds are considered to be the OH (OD) bond of the acid and the OH (OD) bond of a water molecule. The relevant structural parameters of the stretching frequency of the OH bond in 1-naphthol and bond dissociation energy are presented in Table 1 and the excitation energies and m values in Table 2. The ionisation and electronic affinity energies of 1-naphthol were not available. Therefore, the parameters of phenol were considered a good approximation and used in the following calculations.

Table 1
Structural data for proton-transfer reactions in naphthols

	ν (cm^{-1})	l (Å)	D_0 (298 K) (kJ mol^{-1})
Naphthols	3654	0.956	362
H_2O	3219	0.958	514

Bond lengths and dissociation energies from [21]. Vibrational frequencies from [22], in the gas phase for naphthol and in the liquid for water. MeOH and EtOH data were taken as identical to that of naphthols, and acetic and formic acids data were taken as identical to water.

The calculated proton-transfer rate constants through Eq. (10), both in the excited and the ground state, are presented in Table 3. For the S_1 state $k_{\mathrm{H}} = 2.5 \times 10^{10}$ s^{-1}, in excellent agreement with experimental data, $k_{\mathrm{H}}(\mathrm{exp}) = 2.5 \times 10^{10}$ s^{-1}. The isotope effect is KIE(calc) = 2.88 to be compared with KIE(exp) = 3.25. All those values do not take into account any tunnelling effect of the H-atom with a mass of unity, because it is close to unity (ca. $\Gamma_{\mathrm{tunnel}} = 1.2-1.5$).

Parr electrophilicity parameter was estimated through Eq. (7) with the data presented in Table 2, leading to $m = 2.878$ for S_1 of 1-naphthol. No charge-transfer states are involved because m is controlled by the electrophilicity of a single atom (O-atom). Thus, this kind of proton-transfer reaction is better characterised as the transfer of a neutral H-atom, rather than the transfer of a proton. The low barrier of the proton transfer, $\Delta H^{\ddagger} = 9.1$ kJ mol^{-1}, is mainly due to the high value of m, owing to the effect of the excitation energy 0–0 value in S_1. Without such an electronic energy contribution, the index of Parr would be $m = 1.722$ and $\Delta H^{\ddagger} = 26.0$ kJ mol^{-1}. This effect is comparable to that of the reaction energy assessed in terms of pK_a*s, because it increases the rate by ca. 500 times.

The calculations for 2-naphthol are also presented in Table 3 and are in good agreement with experiment.

3.2. Cyano-naphthols

Tolbert and Haubrich [13,14] have reported the synthesis of a new class of photoacids, the cyano derivatives of 1- and

Table 2
Excitation energy and Parr electrophilicity parameter for proton-transfer reactions

	1N/2N (S_0)	1N (S_1)	2N (S_1)	5C1N1	5C2N	6C2N	7C2N	8C2N	DC2N	HPTS
E_e (eV)	–	3.838	3.757	3.444	3.378	3.594	3.374	3.284	3.959	3.757
m	1.722	2.878	2.823	2.613	2.576	2.705	2.574	2.525	2.375	2.823

$I = 8.49$ eV, $A = 2.253$ eV [21]. Excitation energies estimated from [7].

Table 3
Proton transfer in substituted naphthols (and some other similar systems) in excited S_1 states excepted where stated data for ground states S_0

System	ΔpK	ΔG° (kJ mol^{-1})	k_H(exp) (s^{-1})	k_H(calc) (s^{-1})	KIE(exp)	KIE(calc)
1-Naphthol (S_0) + H_2O	10.94	59.3	≈10	4.5	–	–
1-Naphthol (S_1) + H_2O	2.15	9.5	2.5×10^{10}	2.5×10^{10}	3.25	2.88
1-Naphthol (S_1) + acetate	−5.10	−28.9	8×10^{10}	1.1×10^{11}	–	–
1-Naphthol (S_1) + formate	−4.10	−23.2	4.0×10^{10}	9.3×10^{10}	–	–
1-Naphthol-2-sulphonate + H_2O	1.78	16.1	8.8×10^{9}	2.4×10^{9}	2.75	2.58
1-Naphthol-3,6-disulphonate + H_2O	3.32	7.4	5.8×10^{10}	5.0×10^{10}	–	–
2-Naphthol (S_0) + H_2O	11.16	60.8	36	2.7	–	–
2-Naphthol (S_1) + H_2O	4.46	22.6	1.0×10^{8}	2.2×10^{8}	2.56	2.48
2-Naphthol (S_1) + acetate	−1.90	−10.8	2.5×10^{10}	4.9×10^{10}	–	–
5-Cyano-1-naphthol + H_2O	4.47	−8.2	1.3×10^{11}	1.8×10^{11}	1.60	2.39
5-Cyano-1-naphthol + MeOH	−1.43	−8.1	2.6×10^{9}	4.2×10^{10}	2.60	3.00
5-Cyano-1-naphthol + acetate	−7.50	−42.5	1.2×10^{11}	1.0×10^{11}	–	–
5-Cyano-2-naphthol + H_2O	0.99	−2.9	7.0×10^{10}	1.1×10^{11}	2.33	4.01
5-Cyano-2-naphthol + MeOH	2.58	14.6	2.2×10^{8}	1.2×10^{8}	2.27	3.43
6-Cyano-2-naphthol + H_2O	1.37	5.0	1.1×10^{10}	7.0×10^{10}	3.33	3.47
7-Cyano-2-naphthol + H_2O	1.53	5.9	5.5×10^{9}	3.1×10^{10}	3.06	3.47
8-Cyano-2-naphthol + H_2O	1.34	4.8	2.7×10^{10}	4.0×10^{10}	2.08	3.76
5,8-Dicyano-2-naphthol + MeOH	−0.37	−2.1	1.3×10^{10}	3.9×10^{10}	–	–
5,8-Dicyano-2-naphthol + EtOH	−0.33	−1.9	6.3×10^{9}	3.4×10^{10}	–	–
2-Naphthol-6-sulphonate + H_2O	3.69	18.2	1.0×10^{9}	1.0×10^{9}	–	–
2-Naphthol-6,8-disulphonate + H_2O	1.87	7.9	1.7×10^{10}	3.6×10^{10}	–	–
2-Naphthol-3,6-disulphonate + H_2O	2.45	11.2	5.8×10^{8}	1.2×10^{10}	3.62	2.81
6-Br-2-naphthol + H_2O	4.84	24.5	7.2×10^{8}	1.0×10^{8}	–	–
6-CH_3-2-naphthol + H_2O	6.14	31.8	1.3×10^{7}	7.5×10^{6}	–	–
7-CH_3-2-naphthol + H_2O	5.44	27.8	1.6×10^{7}	3.1×10^{7}	–	–
1-Cl-2-naphthol + H_2O	3.44	16.8	4.9×10^{8}	1.6×10^{9}	–	–
1-Hydroxypyrene + acetate	−0.6	−3.40	2.0×10^{9}	2.6×10^{10}	–	–
1-Hydroxypyrene + formate	0.4	2.27	1.6×10^{9}	1.5×10^{10}	–	–
Hydroxypyrene-trisulphonate + H_2O	3.02	14.4	8.0×10^{9}	3.8×10^{9}	4.71	2.68
Hydroxypyrene-trisulphonate + acetate	−4.7	−26.6	7.0×10^{10}	9.7×10^{10}	–	–
Hydroxypyrene-trisulphonate + formate	−3.7	−21.0	6.0×10^{10}	7.0×10^{10}	–	–

Data in water, excepted where stated otherwise: for 1-napthol [12,23]; 5-cyano-1-naphtol [15]; 5, 6, 7 and 8-cyano-1-naphthol [16]; 5-cyano-2-naphtol in water and methanol [24]; 5,8-dicyano-2-naphthol [25–27]; 5-cyano-1-naphthol, 1- and 2-naphthol, 1-hydroxypyrene-trisulphonate (HPTS) and 1-hydroxypyrene (HP) in acetate and 1-naphthol, HPTS and HP in formate [28]; 2-naphtol ground state (GS) and S_1, 2-naphthol-6-sulphonate, 2-naphthol-3,6-disulphonate [29].

2-naphthol, which exhibit excited state acidities in the first singlet state which are comparable to strong mineral acids $pK_a^* = -4 \pm 1$. Pines et al. [15] have reported experimental studies in the ultrafast ESPT of 5-cyano-1-naphthol (5C1N) to water and methanol solutions. In water the Förster cycle calculations lead to an excited state about $pK_a^* = -2.8$ and a dynamic value of $pK_a^* = -2.73$. The proton dissociation time of 5C1N in water was found to be 8 ± 1 ps at 25 °C, one of the fastest dissociation times ever measured, and KIE is ca. 1.6. In methanol the dissociation rates are 2 orders of magnitude lower ($\tau_H = 390$ ps) and KIE is higher (KIE ≈ 2.4).

With the same structural parameters as for 1-naphthol and the experimental $pK_a* = -2.73$, in H_2O the system has a very small barrier ($\Delta H^{\ddagger} \approx 5$ kJ mol^{-1}) and the calculated rate is $k_H = 2.4 \times 10^{11}$ s^{-1} in terms of the transition state theory (Eq. (10)); the experimental value is k_H(exp) = 1.25×10^{11} s^{-1}. The KIE is estimated to be KIE = 2.4 to be compared with KIE(exp) = 1.6.

For methanol the potential energy curves of reactant and product are equal and the estimated rate constant k_H(calc) = 6.3×10^{10} s^{-1} is one (ca.) order of magnitude higher than experiment, k_H(exp) = 2.6×10^{9} s^{-1}. It is important to realise that if the potential energy curves were the same as for reactions in water, the calculated rates would be more than 2 orders of magnitude higher than experiment.

Huppert et al. [16] have also studied ESPT in cyano-substituted 2-naphthols. Table 2 presents the corresponding calculations. With the same structural parameters as in previous examples, with 8-cyano-2-naphthol (8C2N) in water there is a reasonable agreement both for the thermal-activated rates and KIE. With 5C2N, 6C2N and 7C2N, the agreement for the experimental rates is within a factor of three times. The agreement for the rate in methanol is also good. The calculated rate constants for 5,8-dicyano-2-naphthol in methanol and in ethanol are a factor of 6.5–10 times higher than experimental rates (Table 3).

4. Free-energy relationships and other patterns of reactivity

Fig. 3 presents the plot of the calculated rates for fast and ultrafast proton transfers in excited states of several

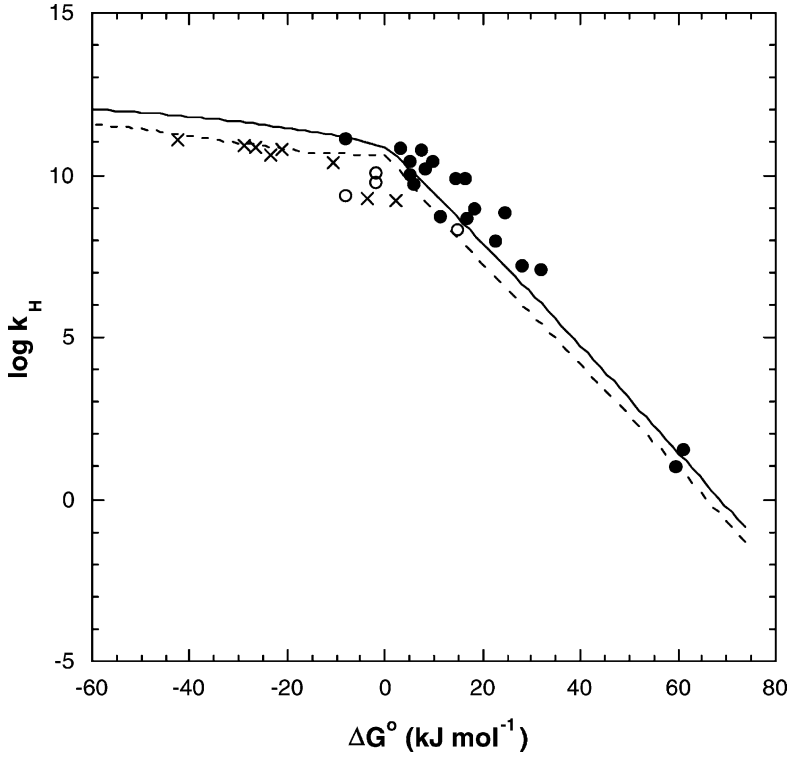

Fig. 3. Plot of $\log k_H$ as a function of reaction energy, ΔG°, for proton-transfer reactions of S_1 in naphthols and substituted naphthols. In water: experimental points (●) and family curve in solid line with $[H_2O] = 55.6\,\text{mol dm}^{-3}$. In alcohols: experimental points (○) and family curve in dashed line, in methanol with $[CH_3OH] = 24.7\,\text{mol dm}^{-3}$. In acetates (×) and $[CH_3COO^-] = 8\,\text{mol dm}^{-3}$.

naphthols and substituted naphthols to water, methanol, ethanol, acetate and formate compiled in Table 3. Families of reactions have to be estimated with the same set of vibrational frequencies, *m* values and acceptor concentrations. Fig. 3 presents the family curves for water and methanol. For each family, data appear to follow a good free-energy relationship, albeit with a sudden change in slope at $\Delta G^{\ddagger} = 0$. This is not due to the presence of any diffusion-controlled plateau, since one is dealing with first-order reactions.

Modern theories on ultrafast proton transfers assume that the transfer of the H-atom in aqueous solution is closely coupled with solvent motion and solvent relaxation and this mechanism can be invoked to account for such a change in slope. However, the present interpretation is associated with the behaviour of the vibrationally adiabatic energy profiles at zero-reaction energy. There is a loss of zero-point energy near the linear transition state because it has only three vibrational modes (one symmetric stretching and two degenerate bendings). This can originate a local minimum in the vibrationally adiabatic surface when a light atom is transferred between two heavy atoms. This minimum is only partially compensated by the increase in entropy, as presented in Appendix A.

Naphthols constitute a very important class of photoacids with rates of proton transfer to several acceptors ranging from femtoseconds in excited states to seconds in ground states. It may come as a surprise that ISM can estimate such a large range of rates (ca. 12 orders of magnitude) in an absolute manner and in good quantitative agreement with experiment (Fig. 4; correlation coefficient $r = 0.98$ and slope 1.09). A few exceptions are found, for example, with 5C1N in methanol and for 6C2N in water. One has to realise that the index of Parr can be slightly different for the substituted naphthols and can also be weakly solvent dependent, notably when charge-transfer rather than atom-transfer mechanism dominates in the index *m*. In principle, all those changes can lead to different rates and, although this does not appear to be the case with naphthols, those factors may be relevant for other systems.

As shown in Table 3, ISM accounts well not only for the changes in the excited-states reactivity, but also for ground states. The increase in proton-transfer rates upon excitation to S_1 by 5×10^9–5×10^7 times for 1- and 2-naphtol in water, respectively, is due not only to a strong decrease in ΔG° but also to an increase in *m*.

Nuclear tunnelling appears to play no significant role on the present systems, but zero-point energies play a major role on the reactivity patterns, both for KIE (Fig. 5) and also for the slopes of the free-energy relations. ISM accounts in reasonable terms for the maximum $KIE_{max} = 4.7$ close to zero-reaction energy. The value of KIE = 4.7 for HPTS in water is close to this estimated value, although the reaction is endothermic ($\Delta G^\circ = 14.4\,\text{kJ mol}^{-1}$). We remark that the pK_a^* of HPTS was taken from Förster cycle.

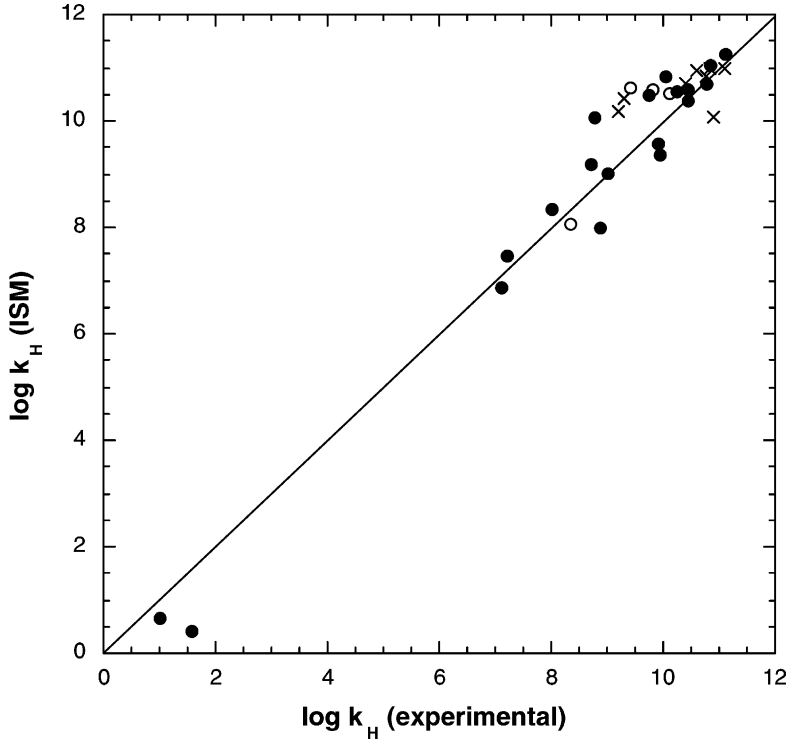

Fig. 4. Correlations between calculated and experimental rate constants, k_H, for proton-transfer reactions in naphthols and substituted naphthols. Solid line: the ideal correlation line. Experimental data for reactions in water (●), in alcohols (○) and in acetates (×).

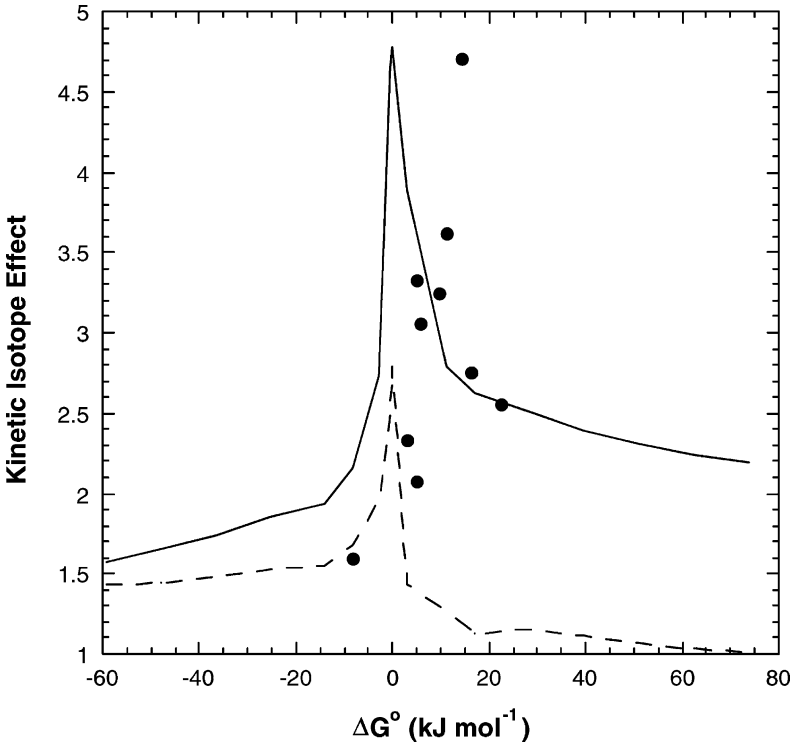

Fig. 5. Calculated KIE: solid line for symmetrical reaction in water; dashed line unsymmetrical case with potential energy curve of naphthol in reactants and that of water in products.

Fig. 5 illustrates an interesting pattern of reactivity, related with the existence of two plateaus around the maximum value. The slope and the relative values of those plateaus depend on the symmetric or asymmetric nature of the potential energy curves of reactant and product. The maximum KIE_{max} values increase with an increase in OH frequencies, due to the increase of zero-point energies. For example, in the symmetrical situation for water/water is $KIE_{max} = 2.8$ and for naphthol/naphthol is $KIE_{max} = 13.9$.

We have shown that a simple semi-classical model as the ISM can give a reasonable approximation to the full quantum–mechanical calculations for proton transfers in naphthols, by relating reaction rates to energetics and to electronic parameters.

Acknowledgements

The authors thank Fundação para a Ciência e a Tecnologia and Sapiens Programme (European Union) for financial support (project no. POCTI/42536/QUI/2001). M.B. acknowledges Fundação para a Ciência e a Tecnologia for financial support (Grant BD/1332/2000).

Appendix A

The variation of the zero-point energy along the reaction path was estimated using the zero-point energies of the BC bond, of the AB bond and of the transition state, and a function with the correct asymptotic limits to interpolate between them. The frequencies of the BC and AB bonds were taken from of the experimental data on phenol and on H_2O in the liquid phase, respectively. The transition state is assumed to be triatomic and linear. Thus, it has one symmetric stretching and two degenerate bendings. The antisymmetric stretching corresponds to the reaction co-ordinate. An approximate solution to stretching frequencies, w, of a linear triatomic molecule can be obtained from the equation of Wilson neglecting cross terms and interactions with the bendings [17]

$$w_{\pm} = \frac{f_{11}(\mu_C + \mu_B) + f_{22}(\mu_A + \mu_B) \pm \sqrt{(f_{11}\mu_C - f_{22}\mu_A)^2 + (f_{11} + f_{22})^2\mu_B{}^2 + 2(f_{11} - f_{22})(f_{11}\mu_C - f_{22}\mu_A)\mu_B}}{2} \tag{A.1}$$

where $\mu_i = 1/m_i$ and f_{11} and f_{22} are the force constants for the BC and AB fragments of the triatomic molecule. In the reactants $f_{11} = f_{BC}$ and $f_{22} = 0$ and in the products $f_{11} = 0$ and $f_{22} = f_{AB}$. Their intermediate values can be estimated from the relation between the force constant of a fractional bond and its bond order [18]

$$f_{11} = f_{BC}(1-n)^{2a\beta_{BC}}, \quad f_{22} = f_{AB}n^{2a\beta_{AB}} \tag{A.2}$$

where f_{BC} and f_{AB} are the force constants for the BC and AB bonds in the isolated reactants and products, respectively, and $a = 0.26$ is Pauling's constant. The BC stretching in the reactants is transformed into the antisymmetric stretching of the transition state and tends to the AB stretching in the products. This antisymmetric stretching does not contribute to the zero-point energy of the transition state because of its imaginary frequency. Thus, the interpolation function that multiplies the antisymmetric frequency w_+ must have the value of unity at the reactants and products and zero at the transition state of a symmetric reaction. At the same time, the symmetric stretching frequency must have the value of zero at the reactants and products and the value of w_- given by Eq. (A.1) at the symmetrical transition state. A function that obeys the above conditions is

$$f(n) = \frac{1}{\cosh[-a' l_{BC,eq}\ln(n^{\ddagger})/l_{AB} - l_{AB}(n=0.5)]},$$
$$\text{for } 0 < n < 0.5;$$
$$f(n) = \frac{1}{\cosh[-a' l_{AB,eq}\ln(1-n^{\ddagger})/l_{BC} - l_{BC}(n=0.5)]},$$
$$\text{for } 0.5 < n < 1 \tag{A.3}$$

with $n^{\ddagger}$ representing the bond order of the classical transition state. The symmetric and antisymmetric stretching can now be obtained making

$$\nu_{sym} = \frac{1}{2\pi c}\sqrt{w_-}[1 - f(n)],$$
$$\nu_{asym} = \frac{1}{2\pi c}\sqrt{w_+}f(n) \tag{A.4}$$

The calculation of the enthalpy of activation according to Eq. (11) presumes the use of the classical potential energy and of the zero-point energy at the configuration where the free energy attains its maximum. This requires information on the variation of the entropy along the reaction co-ordinate. The entropy associated with the vibrations is given by the standard statistical mechanical equation

$$S_v = R\left\{\frac{\theta_v/T}{\exp(\theta_v/T) - 1} - \ln\left[1 - \exp(-\theta_v/T)\right]\right\} \tag{A.5}$$

where θ_v is the vibrational temperature. The variation of vibrational entropy is the difference between the entropy of the symmetric stretching plus the two bending, minus the BC stretching. This difference is multiplied by $1 - f(n)$, just like ν_{sym} in Eq. (A.4), to account for the variation of the vibrational entropy along the reaction co-ordinate.

The variation of translational entropy is determined by the difference of translational entropy of the transition state (one triatomic molecule) and that of the reactants (one diatomic molecule and one atom). The variation of the rotational entropy results from the difference of the moment of inertia between the linear transition state and the diatomic molecule

in the reactants. Standard equations were employed to calculate the translational and rotational entropies [19]. The variation of these entropies along the reaction co-ordinate was modelled by a function similar to Eq. (A.3),

$$f(n) = \frac{1}{\cosh[-a' l_{\mathrm{BC,eq}} \ln(n^{\ddagger})/l_{\mathrm{AB}} - l_{\mathrm{AB}}^{\ddagger}]},$$

for $l_{\mathrm{AB}} < l_{\mathrm{AB}}^{\ddagger}$;

$$f(n) = \frac{1}{\cosh[-a' l_{\mathrm{AB,eq}} \ln(1-n^{\ddagger})/l_{\mathrm{BC}} - l_{\mathrm{BC}}^{\ddagger}]},$$

for $l_{\mathrm{BC}} < l_{\mathrm{BC}}^{\ddagger}$

with the difference that now the asymptotic limit is not $n = 0.5$, but the classic transition state configuration. This choice was motivated by the fact that the thermodynamic functions, and in particular the entropy, are only defined at positions of mechanical equilibrium, such as at the reactants and at the classical transition state [20]. For the same reason, we resist the temptation of defining a free-energy profile. However, Fig. 2 illustrates the variation of the entropy along the reaction co-ordinate, because it is relevant to locate the position where the values of $\Delta V^{\ddagger}$ and $\Delta Z^{\ddagger}$ must be calculated in order to obtain $\Delta H^{\ddagger}$ according to Eq. (11).

Finally, $\Delta S^{\ddagger}$ can be calculated from its different components. Its value can be used together with that of $\Delta H^{\ddagger}$ to calculate $\Delta G^{\ddagger}$, and the thermodynamic formulation of transition state theory can be used. The pre-exponential factor obtained with this method is ca. 5 times lower than the value of $10^{10}\,\mathrm{M^{-1}\,s^{-1}}$ employed in our calculations. The calculated pre-exponential factor seems to be too low in view of the collision frequency in solution, $10^{11}\,\mathrm{M^{-1}\,s^{-1}}$, and reflects the limitations of using equations derived for the gas phase to reactions in solution. The constant value of $10^{10}\,\mathrm{M^{-1}\,s^{-1}}$ is a good compromise between the gas phase calculations and the solution behaviour.

References

[1] A.J.C. Varandas, S.J. Formosinho, J. Chem. Soc., Faraday Trans. 2 (82) (1986) 953.
[2] L.G. Arnaut, S.J. Formosinho, J. Phys. Chem. 92 (1988) 685.
[3] L.G. Arnaut, S.J. Formosinho, J. Photochem. Photobiol. A: Chem. 75 (1993) 1.
[4] L.G. Arnaut, A.A.C.C. Pais, S.J. Formosinho, J. Mol. Struct. 563/564 (2001) 1.
[5] L.G. Arnaut, A.A.C.C. Pais, S.J. Formosinho, J. Chem. Phys., submitted for publication.
[6] R.G. Parr, L.V. Szentpály, S. Liu, J. Am. Chem. Soc. 121 (1999) 1922.
[7] L.M. Tolbert, K.M. Solntsev, Acc. Chem. Res. 35 (2002) 19.
[8] H.S. Johnston, C. Parr, J. Am. Chem. Soc. 85 (1963) 2544.
[9] N. Agmon, R.D. Levine, J. Chem. Phys. 71 (1979) 3034.
[10] L. Pauling, J. Am. Chem. Soc. 69 (1947) 542.
[11] B.C. Garrett, D.G. Truhlar, J. Phys. Chem. 83 (1979) 2921.
[12] E. Pines, D. Tepper, B.-Z. Magnes, D. Pines, T. Barak, Ber. Bunsen-Ges. Phys. Chem. 102 (1998) 504.
[13] L.M. Tolbert, J.E. Haubrich, J. Am. Chem. Soc. 112 (1990) 8163.
[14] L.M. Tolbert, J.E. Haubrich, J. Am. Chem Soc. 116 (1994) 10593.
[15] E. Pines, D. Pines, T. Barak, B.-Z. Magnes, L.M. Tolbert, J.E. Haubrich, Ber. Bunsen.-Ges. Phys. Chem. 102 (1998) 511.
[16] D. Huppert, L.M. Tolbert, S. Linares-Samaniego, J. Phys. Chem. A 101 (1997) 4602.
[17] E.B. Wilson Jr, J. Chem. Phys. 7 (1939) 1047.
[18] H.-B. Burgi, J.D. Dunitz, J. Am. Chem. Soc. 109 (1987) 2924.
[19] D.A. McQuarrie, Statistical Mechanics, Harper & Row, New York, 1976.
[20] E. Grunwald, Prog. Phys. Org. Chem. 17 (1990) 55.
[21] Handbook of Chemistry and Physics, 3rd Electronic Edition, CRC Press Inc., 2001.
[22] http://webbook.nist.gov/chemistry/
[23] S.P. Webb, L.A. Philips, S.W. Yeh, L.M. Tolbert, J.H. Clark, J. Phys. Chem. 90 (1986) 5154.
[24] K.M. Solntsev, D. Huppert, N. Agmon, L.M. Tolbert, J. Phys. Chem. A 104 (2000) 4658.
[25] B. Cohen, D. Huppert, J. Phys. Chem. A 105 (2001) 2980.
[26] I. Carmeli, D. Huppert, L.M. Tolbert, J.E. Haubrich, Chem. Phys. Lett. 260 (1996) 109.
[27] B. Cohen, D. Huppert, J. Phys. Chem. A 104 (2000) 2663.
[28] E. Pines, B.-Z. Magnes, M.J. Lang, G.R. Fleming, Chem. Phys. Lett. 281 (1997) 413.
[29] M. Gutman, E. Nachliel, Biochim. Biophys. Acta 1015 (1990) 391.